3D PiC code investigations of Auroral Kilometric Radiation mechanisms

K.M. Gillespie[1], S.L. McConville[1], D.C. Speirs[1] , K. Ronald[1], , A.D.R. Phelps[1], R. Bingham[1,2], A.W. Cross[1], C.W. Robertson[1], C.G. Whyte[1], W. He[1], I. Vorgul[3], R.A. Cairns[3] and B.J. Kellett[2]

[1]SUPA Department of Physics, John Anderson Building, 107 Rottenrow, University of Strathclyde, Glasgow, G4 0NG, Scotland

[2] Space Science and Technology Department, STFC Rutherford Appleton Laboratory, Didcot, OX11 0QX, England

[3] School of Mathematics and Statistics, University of St Andrews, St Andrews, KY16 9SS, Scotland

Email - karen.gillespie@strath.ac.uk

Abstract. Efficient (~1%) electron cyclotron radio emissions are known to originate in the X mode from regions of locally depleted plasma in the Earths polar magnetosphere. These emissions are commonly referred to as the Auroral Kilometric Radiation (AKR). AKR occurs naturally in these polar regions where electrons are accelerated by electric fields into the increasing planetary magnetic dipole. Here conservation of the magnetic moment converts axial to rotational momentum forming a horseshoe distribution in velocity phase space. This distribution is unstable to cyclotron emission with radiation emitted in the X-mode. Initial studies were conducted in the form of 2D PiC code simulations [1] and a scaled laboratory experiment that was constructed to reproduce the mechanism of AKR. As studies progressed, 3D PiC code simulations were conducted to enable complete investigation of the complex interaction dimensions. A maximum efficiency of 1.25% is predicted from these simulations in the same mode and frequency as measured in the experiment. This is also consistent with geophysical observations and the predictions of theory.

1. Introduction

Electrons precipitating into the Earth's magnetosphere, Figure 1, are subject to increasing magnetic field with decreasing altitude. In the absence of collisions and given that the field increases slowly compared to the electron oscillation period, the adiabatic conservation of the magnetic moment comes into effect. Electrons entering the Earth's magnetic dipole structure have a spread in their initial velocity. Those electrons having a small initial component of velocity perpendicular to the magnetic flux lines experience an increase in their rotational component of velocity as they descend towards the atmosphere. The effect of this process is that an initially primarily rectilinear electron beam assumes a

horseshoe formation in electron velocity space with a significant number of electrons having high pitch angles $\theta = \arctan(v_{\perp}/v_{//})$ and a region with a positive gradient in number density vs perpendicular velocity, $dn/dv_{\perp}$, Figure 2. Such horseshoe electron distributions have been measured in the AKR source regions within the polar magnetosphere [2-3].

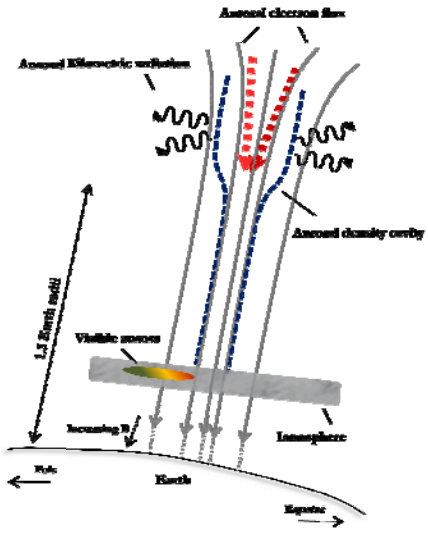

Figure 1: Representation of the AKR source region and terrestrial auroral process.

Part of the electron stream is 'mirrored', reversing its direction of motion along the magnetic field lines once all of its kinetic energy becomes associated with rotational motion providing a second energetic electron population in the auroral magnetosphere, the space bound component. Due to the correlation between the electron cyclotron frequency and the radio frequency, it has been hypothesized for some time that the emissions are due to a cyclotron instability [4-7] in one or both of these populations [8-13].

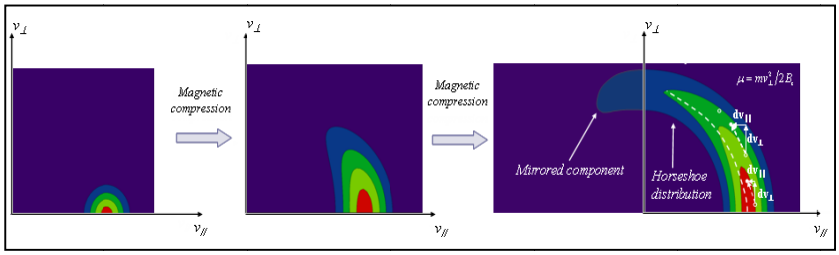

Figure 2 : Formation of the horseshoe in the electron velocity distribution

Over the last few decades, as technology has advanced satellites have been able to obtain quantitative data on the phenomenon of Auroral Kilometric Radiation [14,15]. The magnetospheric measurements have revealed that the radiation emissions are sourced in regions of plasma depletion ($\omega_{pe}<<\omega_{ce}$) at an altitude of 1.5-3 Earth radii. The frequency observed at any given altitude extends down to the local electron cyclotron frequency with the strongest emission at around 300kHz. The wave propagation and polarisation directions suggest that the radiation is generated in the X-mode

[16] with a peak power ~10^9 W, corresponding to an estimated radiation efficiency ~1% of the auroral electron precipitation energy [2,3]. The availability of accurate data has resulted in a significant research effort to explain the unusually high efficiency of this natural process. This enhanced data allows for meaningful comparison with theoretical expectations and has resulted in a number of models for the emission mechanisms.

As the equations describing this instability scale with the cyclotron frequency, it became clear that it would be possible for the concept to be tested in a laboratory experiment by increasing the magnetic flux density and scaling the resonance into the microwave regime. In conjunction with the construction of an experimental reproduction of the AKR source region, 2D PiC simulations were conducted. Those simulations have demonstrated the formation of horseshoe distribution in an electron-beam subject to significant magnetic compression and subsequent cyclotron maser emission within an interaction waveguide. [1,17] Although the experimental results [18] were in good agreement with the findings from the 2D PiC simulations, certain aspects of the experimental behavior results require 3D computational approaches for reproduction. Specifically 2D simulations cannot account for an azimuthal index in the modes propagating in the waveguide, aspects of the experimental behavior associated with such modes require 3D simulations. This enhanced numerical simulation work will be used to redesign the laboratory experiment in the future. This paper presents most recent results from simulations conducted in three dimensions.

2. 3D PiC CODE SIMULATIONS

2.1. Simulation objective

2D PiC code simulations provide high execution speed and strong numerical stability. However, 2D simulations although in good agreement with the experiment, can only allow for generation of axisymmetric modes, which means that modes with azimuthal structure cannot be predicted. In conducting 3D simulations a more complete interaction regime may be analysed [19]. The 2D simulations were conducted for electron beam energies of 75-85keV, magnetic compression factors of up to 30 and electron cyclotron frequencies of 4.42GHz and 11.7GHz. At 11.7GHz, beam-wave coupling was observed with the $TE_{0,3}$ mode and an RF output power of 20kW was predicted corresponding to an RF conversion efficiency of 1.3%. At 4.42GHz, excitation of the $TE_{0,1}$ mode was observed with an RF output power of 35kW for a cyclotron-wave detuning of 2%. This corresponds to an RF conversion efficiency of 2.6%. The RF conversion efficiencies obtained are therefore comparable with estimates for the AKR generation efficiency [14]. The 3D simulation geometry, Figure 3, illustrates the main interaction waveguide with a predefined electron horseshoe distribution injected. The gun geometry is not modeled due to the computational requirements of 3D simulations. A uniform axial magnetic field profile was defined from 0-20cm with a linear decrease to 0T from 20-80cm as an initial condition for the PiC code. Recent 3D simulations have been used to study the excitation of modes in the two resonance regimes, which provides data to compare with experimental measurements and illustrate mode competition that 2D simulations were not able to account for.

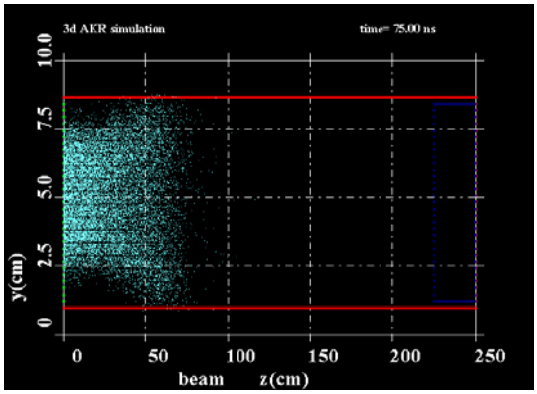

Figure 3: Simulation geometry illustrating waveguide with electron beam PiC particle trajectory, and pre-defined horseshoe distribution.

2.2. Mode analysis

3D simulations plot transverse electric field patterns within the waveguide interaction region. Figure 4(a) illustrates the results of the transverse spatial Fourier analysis output from 3D KARAT for the 11.7GHz resonance, illustrating a $TE_{2,3}$ mode pattern. It is very clear that the simulation also has predicted a strong coupling with the $TE_{0,3}$ mode, Figure 4(b) (a transverse spatial Fourier analysis) and Figure 5(a), along with a few other weaker couplings. These modes were observed in the experimental measurements for this resonance regime. Further analysis of the simulations have been undertaken to study how different factors such as the beam current and the cyclotron detuning affects the modes being excited within the interaction region, and the resultant output power. The detuning is measured as a fractional shift of the cyclotron frequency from the cut-off of the $TE_{0,3}$ mode.

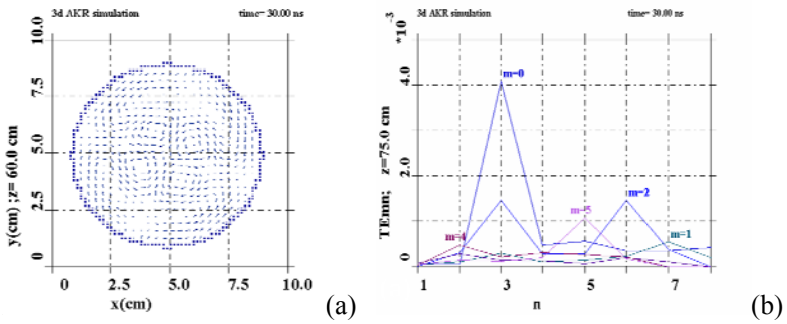

Figure 4: (a) 3D vector predictions of the transverse electric field patterns within the waveguide interaction region, the structure of a $TE_{2,3}$ mode is clearly seen at 11.7GHz. (b) illustrates the results of the transverse spatial Fourier analysis output predicted by KARAT 3D for the 11.7GHz resonance.

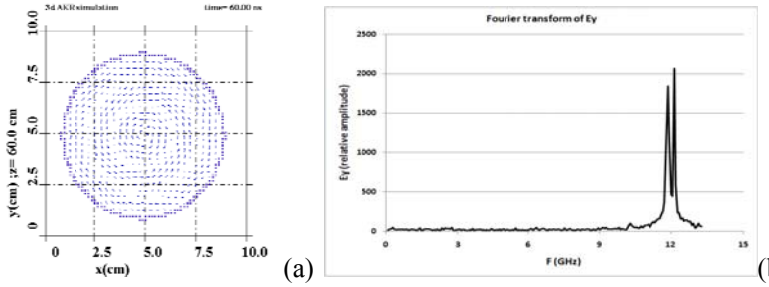

(a) (b)

Figure 5: (a) Illustrates excitation of $TE_{0,3}$ mode. (b) shows a peak at ~11.7GHz along with another at ~12.2GHz, this is illustrative of multiple modes being excited and mode competition.

2.3. Mode competition and Power output

A clear trend was observed throughout the plots, when the beam current becomes lower the average power output decreased. The range of predicted output powers were comparable with the findings from 2D simulations & experimental measurements. The RF output power increased with detuning below resonance but decreased with detuning above resonance. When the detuning was set below resonance the peak power output was high, and the recurring dominant mode was the $TE_{2,3}$. When the detuning increased above resonance the recurring mode excited was the $TE_{0,3}$ whilst the output power decreased. It was noticed that mode competition was more severe as the detuning increased above resonance. Figure 5(b) shows a clear peak at ~11.7GHz, in agreement with the experimental results, along with another at ~12.2GHz, this is illustrative of multiple modes being excited and mode competition. For a beam current of 37A, the predicted RF power output was in the range 40-180kW for a detuning of -3 to 3%. This corresponds to an RF conversion efficiency of ~1-6%, which is comparable with the 2D simulations and experiments. Figure 6(a) illustrates a Poynting flux integral predicted by simulations of the 11.7GHz resonance regime, showing output power rising to 25kW, with a beam current of 13A.

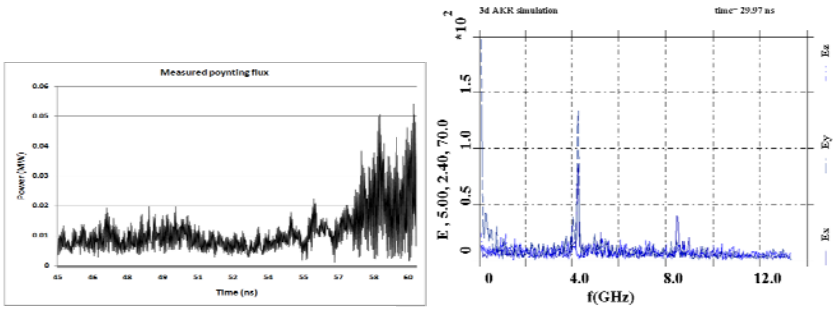

(a) (b)

Figure 6: (a) illustrates a Poynting flux integral for the 11.7GHz resonance regime (b) illustrates some of the initial results taken from the simulations, at 4.42GHz resonance.

These results are comparable with that the experimental measurements, [20-22] and also with the auroral source region, where the radiation spectra has shown detailed structure. Simulations at the

resonance at 4.42GHz, are ongoing to study it dynamics in three dimensions. From initial results, the 3D simulations are also proving successful in simulating this resonance regime. Figure 6(b) illustrates some of the initial results taken from the simulations, cleary showing the spectral components measured in experimental data, a large peak at 4.42GHz and a small second harmonic at 8.5GHz.

3. CONCLUSION AND DISCUSSIONS

In summary, it has been shown that the 3D PiC codes are useful in simulating the interaction between a complex electron beam and electromagnetic radiation. These new simulations have proven accurate in identifying the modes and the mode competition that existed in experiment. The peak powers also agree well with those predicted in the experiment and previous simulations.

This enhanced picture of the interaction region will prove valuable for further studies to improve the understanding of AKR and thus the general field of instability and waves in plasmas [23]. Research will continue with simulations being conducted to refine these results investigating the sensitivity to the exact form of the electron distribution function. Lastly these results will aid in design modifications to the apparatus to experimentally measure the sensitivity to detuning in the laboratory experiment for comparison with theoretical predictions.

References

[1] D.C. Speirs et al, *Plasma Phys. Contol. Fusion* **50** (2008)
[2] R.E. Ergun et al, *Astrophyical Journal* **538** pp456-466 (2000
[3] G.T. Delory et al, *Geophys. Res. Lett*, **25** pp2069-2072 (1998)
[4] R.Q. Twiss, *Aus. J. Phys.* **11** pp564-579 (1958)
[5] A.V. Gaponov 1959 *Izv. VUZ. Radiofizika* **2** pp450-462 and pp837
[6] K.R. Chu, *Rev. Mod. Phys*. **76** pp489-540 (2004)
[7] P. Sprangle & A.T. Drobot, *IEEE Trans. on Microwave Theory and Technique* **MTT-25**
[8] J.S. Wagner et al, *Radio Science* **19** pp509-518 (1984)
[9] C.S Wu & L.C. Lee, *The Astrophysical Journal* **230** pp621-626 (1979)
[10] R. Bingham et al, *Contrib. Plasma Phys.* **44** pp382-387 (2004)
[11] R. Bingham et al, *Physica Scripta* **T98** pp160-162 (2002)
[12] R. Bingham et al, *Phys. Plasmas* **7** pp3089-3092 (2000)
[13] I. Vorgul et al, *Phys. Plasmas* **12** Art. 122903 (2005)
[14] D.A. Gurnett 1974 J. Geophys. Research: Space Physics **79** pp4227-4238
[15] D.B. Melrose et al, *J. Geophys. Research: Space Physics* **87** pp5140-5150 (1982)
[16] R.F. Benson *J. Geophys. Res- Space Physics* **90** pp2753-2784 (1985)
[17] D.C. Speirs et al, *J. Plasma Phys.* **71** pp665-674 (2005)
[18] S.L. McConville et al, *Plasma Phys. Control. Fusion* **50** (2008)
[19] K.M. Gillespie et al, *Plasma Physics & Controlled Fusion* **50**, 124038 (2008)
[20] K. Ronald et al, *Plasma Sources, Science and Technology* **17** (2008)
[21] K. Ronald, *Phys. Plamas.* **15** Art. 056503 (2008)
[22] K. Ronald et al, *IEEE Trans. on Plasma Science* **PS-26** pp375-382 (1998)
[23] J.E. Allen & A.D.R. Phelps, *Rep. Prog. Phys*., **40**, pp1305-1368 (1977)